

Exergoeconomic optimization of an ammonia–water hybrid absorption–compression heat pump for heat supply in a spray-drying facility

Jonas K. Jensen · Wiebke B. Markussen ·
Lars Reinholdt · Brian Elmegaard

Received: 30 October 2014 / Accepted: 12 February 2015 / Published online: 22 February 2015
© The Author(s) 2015. This article is published with open access at Springerlink.com

Abstract Spray-drying facilities are among the most energy intensive industrial processes. Using a heat pump to recover waste heat and replace gas combustion has the potential to attain both economic and emissions savings. In the case examined a drying gas of ambient air is heated to 200 °C yielding a heat load of 6.1 MW. The exhaust air from the drying process is 80 °C. The implementation of an ammonia–water hybrid absorption–compression heat pump to partly cover the heat load is investigated. A thermodynamic analysis is applied to determine optimal circulation ratios for a number of ammonia mass fractions and heat pump loads. An exergoeconomic optimization is applied to minimize the lifetime cost of the system. Technological limitations are imposed to constrain the solution to commercial components. The best possible implementation is identified in terms of heat load, ammonia mass fraction and circulation ratio. The best possible implementation is a 895 kW heat pump with an ammonia mass fraction of 0.82 and a circulation ratio of 0.43. This results in economic savings with a present value of 146,000 € and a yearly CO₂ emissions reduction of 227 ton.

Keywords Spray-drying · Hybrid heat pump · Exergoeconomics · High-temperature heat pump · Ammonia–water · Absorption

Abbreviations

COP	Coefficient of performance
CRF	Capital recovery factor
EES	Engineering equation solver
HACHP	Hybrid absorption–compression heat pump
IHEX	Internal heat exchanger
LMTD	Logarithmic mean temperature difference
PEC	Product equipment cost

Symbols

b	Plate corrugation depth (m)
\dot{C}	Cost rate of exergy flow (€/s)
c	Average cost per unit exergy (€/kJ)
\dot{E}	Exergy flow rate (kW)
e	Specific exergy (kJ/kg)
f	Circulation ratio (–)
f_{ex}	Exergoeconomic factor (–)
h	Specific enthalpy (kJ/kg)
h_{op}	Yearly operating time (s)
L	Plate length (m)
\dot{m}	Mass flow rate (kg/s)
N	Number of (–)
p	Pressure (bar)
\dot{Q}	Heat load (kW)
q	Vapour quality (–)
r	Relative cost difference (–)
s	Specific entropy (kJ/kg-K)
T	Temperature (°C (difference K))
t	Plate thickness (m)
\dot{V}	Volume flow rate (m ³ /s)

J. K. Jensen (✉) · W. B. Markussen · B. Elmegaard
Department of Mechanical Engineering, Technical University
of Denmark, Nils Koppels Alle, Building 403,
2800 Kgs. Lyngby, Denmark
e-mail: jkije@mek.dtu.dk

W. B. Markussen
e-mail: wb@mek.dtu.dk

B. Elmegaard
e-mail: be@mek.dtu.dk

L. Reinholdt
Danish Technological Institute, Kongsvang Alle 29,
8000 Århus, Denmark
e-mail: lre@teknologisk.dk

\dot{W}	Work load (kW)
W	Plate width (m)
x	Ammonia mass fraction (–)
y	Exergy destruction ratio (–)
\dot{Z}	Levelized non-exergetic cost rate (€/s)

Greek

β	Chevron angle (°)
Δ	Difference
ϵ	Effectiveness (–)
ε	Exergy efficiency (–)
η	Efficiency (–)
Λ	Plate corrugation spacing (m)
λ	Thermal conductivity (kW/m-K)

Subscripts

D	Destruction
e	Electric
elec	Electricity cost
F	Fuel
gas	Gas cost
is	Isentropic
j	Stream
k	Component
l	Lean
P	Product
pp	Pinch point
r	Rich
sys	System
v	Vapour
vol	Volumetric

Superscripts

Σ	Sum over all k components
CH	Chemical
OP	Operational costs
PH	Physical

Introduction

Spray-drying facilities are among the most energy intensive industrial processes. They are applied in the production of dry solids from a liquid feedstock. This is typically needed in the chemical, pharmaceutical or food industry. Typical products of spray-drying processes are powdered milk, detergents and dyes. A survey from 2005 [1] showed that the yearly energy consumption for drying operation in the United Kingdom was 348.6 PJ, corresponding to 17.7 % of industrial energy consumption. Spray-drying processes are typically fuelled by fossil fuel combustion, most commonly natural gas [1]. Therefore, spray-drying

facilities are not only accountable for a large energy consumption but also for a large quantity of green house gas emissions. Improving the energy efficiency of spray-drying facilities is thus important to reach the goals for a sustainable development of the industrial sector.

Given the recent and projected increase in renewable electricity generation from sources such as wind and solar [2], moving energy consumption from gas combustion to an electrically driven heat pump could be an environmental benefit.

The implementation of heat pumps in spray-drying facilities is typically restricted by the high temperature of the exhaust air (80–100 °C), which is out of the working domain for most industrial vapour compression heat pumps [3, 4]. The ammonia–water hybrid absorption–compression heat pump (HACHP), however, has several attributes making it applicable for high-temperature operation [3, 5].

The HACHP is based on the Osenbrück cycle [6]. The first theoretical study of which was performed by Altenkirch [7], who described the advantage of the HACHP heat pump with the non-isothermal process of absorption–desorption compared to the isothermal process of condensation–evaporation. Thereby, the cycle approaches the Lorenz cycle [8], which can increase the heat pump efficiency by reducing the entropy generation driven by heat transfer over a finite temperature difference.

Heat pump-driven drying processes has been studied by Prasertsan et al. [9], Gungor et al. [10] and Chua et al. [11]. These investigations have been limited to low-temperature drying processes due to the constrained heat supply temperature of conventional vapour compression heat pumps. The maximum supply temperature of vapour compression heat pumps is bound by the maximum allowable pressure of the compressor technology and the corresponding saturation temperature of the refrigerant [4].

Using a zeotropic mixture as working fluid reduces the vapour pressure compared to the vapour pressure of the pure volatile component. Using the newly developed high pressure ammonia components (50 bar max. pressure) heat supply temperatures up to 150 °C can be achieved using the HACHP [5]. The limit for a pure ammonia system with these components is 90 °C [4]. The development of these high pressure components and their combination with the HACHP technology has thereby shifted the working domain of industrial heat pumps, making it applicable for processes like spray-drying. However, whether this shift allows economic and environmental savings in industry is still unanswered and should be estimated to evaluate whether heat pump development should be moved in this direction.

Ommen et al. [12] presented exergoeconomic optimization of the HACHP. This showed that the HACHP can be competitive with gas combustion and that the HACHP is

the only applicable heat pump technology in the temperature range of the present study. Ommen et al. [12] tested ammonia mass fractions of 0.7 and 0.9 and found the total cost to increase with the reduction of ammonia mass fraction. This assumes constant heat transfer coefficients for the absorption and desorption. It is though well known that the heat transfer coefficient of a refrigerant mixture can be reduced due to either mass diffusion resistance of the volatile component or an unfavourable change in the mixture transport properties [13, 14]. The heat transfer reduction is increased when the mixture composition is moved away from the pure components. This effect is thereby not accounted for in [12]. Satapathy [15] and Hultèn and Berntsson [16, 17] also conclude that the ammonia mass fraction should be as high as possible, [15] concludes this based solely on exergy analysis while [16, 17] conclude this based on an evaluation of both COP and investment.

This paper will investigate the economic and environmental implication of implementing a HACHP in a spray-drying facility. Using detailed heat transfer correlations the effect of changing ammonia mass fraction will be accounted for. The heat pump load, ammonia mass fraction and the circulation ratio in the HACHP will all be analysed and optimized within commercial component constraints. Combination of four ammonia concentrations and four heat pump loads will be investigated. This yields a total of 16 design conditions at which the HACHP design will be optimized.

To optimize the design, an exergoeconomic optimization [18, 19] is applied in each of the 16 conditions. By optimizing the design of each of these 16 conditions, the best possible design can be found and the effect of changing heat pump load and ammonia mass fraction can be evaluated without bias.

The objective of the present work is thus to evaluate if implementing a HACHP in a spray-drying facility is: technically feasible, using current commercial components and further, if such an installation will be economically viable as well as environmentally beneficial.

Methods

Spray-drying facility and heat pump implementation

A generic spray-drying facility, as seen in Fig. 1, was studied. The HACHP was implemented to heat the drying air prior to the gas burner. A detailed overview of the HACHP unit (indicated by the dashed box) is shown in Fig. 2 (left), further the streams from Fig. 2 (left) that are present in Fig. 1 are indicated by the given stream numbers.

The ambient air is introduced to the system by an air blower at a rate of 100,000 m³/h. The air stream is first heated by a fraction of the exhaust air. Hereafter, it is heated by a flue gas heat recovery heat exchanger. The ambient air has a temperature of 20 °C and a humidity ratio of 0.006 kg/kg. At the outlet of the flue gas heat recovery

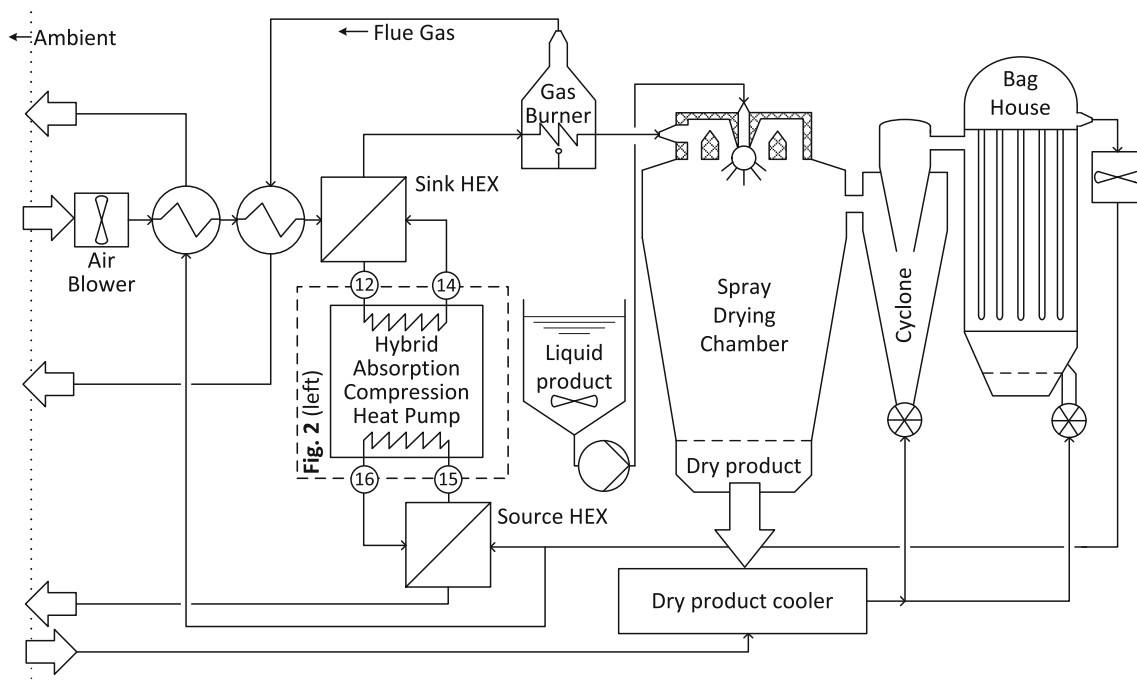


Fig. 1 Principle sketch of the investigated spray-drying facility

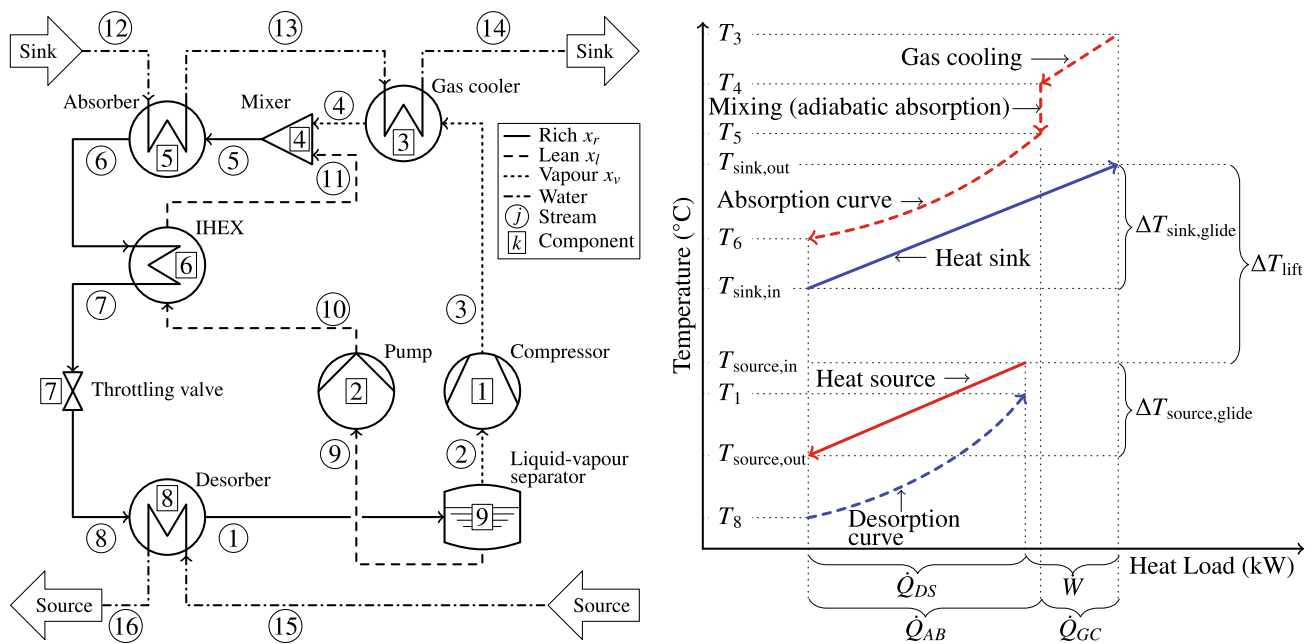


Fig. 2 Left principle sketch of the HACHP, right HACHP heat process sketched in a temperature heat load diagram

heat exchanger, the drying air is 80°C . From here, the drying air is heated by the HACHP, utilizing exhaust air as the heat source. The drying air is then heated to 200°C by a natural gas burner.

Heating the air from 20 to 200°C results in a total heat load of 6.1 MW . The larger the HACHP load, the more of the total heat load will be moved from the gas burner to the HACHP. As the exhaust temperature is uninfluenced by this: the temperature lift supplied by the HACHP increases with increasing load, thus decreasing the coefficient of performance (COP). It is, therefore, necessary to find a suitable HACHP load to ensure the viability of the investment.

When the air has reached the target temperature of 200°C , it enters the spray-drying chamber and is mixed with the atomized stream of the liquid product. This causes the liquid in the product to evaporate. The dry product can then be extracted from the bottom of the chamber. The now more humid air is passed first through a cyclone and then a bag house filter to remove leftover product. Here, air heated by the dry product is introduced. The exhaust air exiting the bag house has a temperature of 80°C , humidity ratio of 0.045 kg/kg and approximately twice the mass flow rate of the drying air. This means that the capacity rate of the exhaust is higher than that of the air being heated. Therefore, the exhaust stream can be split such that half can be used to heat the air directly and the rest can be used as the heat source in the HACHP. This, in combination with the use of a flue gas heat recovery heat exchanger ensures that there is an actual heat surplus at the exhaust air temperature. Consequently, the HACHP as implemented here will transfer heat across the pinch temperature [18].

The analysis and results presented in this paper are only valid for such systems. This is not always the case [20] and as a consequence of pinch analysis [18], the exhaust air is best utilized by heating the incoming air directly.

To reduce the risk of contamination, two secondary circuits are used to transfer the heat between the drying/exhaust air and the HACHP. The heat transfer fluid is water. On the sink side, this is pressurized to prevent evaporation. The secondary circuits will increase the HACHP temperature lift, thus reducing the COP, but is assumed to be a necessary safety measure.

Modelling and analysis of the HACHP

The process diagram of the evaluated HACHP may be seen in Fig. 2 (left). The process is sketched in the temperature–heat load diagram shown in Fig. 2 (right). Here, it may be seen that the profiles of the absorption and desorption processes are non-linear. This has been described in detail by Itard and Machielsen [21]. In Fig. 2, these are depicted as convex curves. Dependent on the ammonia mass fraction and circulation ratio, these profiles could also exhibit a concave curve or have a convex and a concave part. This is well described in Zheng et al. [22]. Therefore, when modelling the HACHP, it is not sufficient to ensure a positive temperature difference at the inlet and outlet of the absorber and desorber. To ensure a feasible profile, it is necessary to verify that there is a positive temperature difference over the entire heat transfer process.

A numerical model of a HACHP has been developed in Engineering Equation Solver (EES) [23]. The

thermodynamic properties of the ammonia–water mixture were calculated using equations of state developed by Ibrahim and Klein [24]. Transport properties were calculated using the correlation developed by El-Sayed [25], as suggested by Thorin [26]. Each component was modelled based on a steady state mass and energy balance. Further, the model ensured that the second law was fulfilled in all components.

The rich ammonia mass fraction, x_r , and circulation ratio, f , were inputs to the model. The rich ammonia mass fraction is present in state 5–8 and 1. The circulation ratio was defined as the ratio between the mass flow rate of the rich solution, \dot{m}_r , and the lean solution, \dot{m}_l :

$$f = \frac{\dot{m}_l}{\dot{m}_r} \tag{1}$$

Hence, the circulation ratio was directly linked to the vapour quality in state 1, exiting the desorber, such that: $q_1 = 1 - f$. From this it can be concluded that if, $f = 0$ then, the HACHP is essentially a vapour compression heat pump with a zeotropic working fluid.

Pressure and heat losses in the liquid/vapour separator were neglected, hence the temperature and pressure of stream 2 and 9 were the same as stream 1. It was assumed that the vapour and liquid exiting the separator were saturated, $q_2 = 1$ and $q_9 = 0$. The vapour and lean ammonia mass fraction, x_v and x_l , were then determined by equilibrium. The processes in the compressor and pump were modelled as adiabatic with given isentropic efficiencies, η_{is} . The transferred heat in the internal heat exchanger (IHEx) and gas-cooler was calculated based on given values of effectiveness, ϵ .

The mixing or adiabatic absorption process, found prior to the absorber, was modelled as an isobaric process by a mass and energy balance. Thus, state 5 was the equilibrium state attained when mixing stream 4 and 11. The state exiting the absorber was assumed to be saturated, $q_6 = 0$. The forced adiabatic expansion in the throttling valve was assumed to be isenthalpic, $h_7 = h_8$.

The high and low pressures, p_H and p_L , were determined to satisfy given values of pinch-point temperature difference, ΔT_{pp} , in the absorber and desorber. As enthalpy and temperature are not proportional during the process of absorption and desorption, these processes were discretized in heat load, giving the temperature of the water and the ammonia–water mixture and thus, the temperature difference at each step. The pinch-point temperature difference was defined as the minimum of these. Thirty steps were used for both the absorber and desorber.

The COP of the HACHP was defined as given in Eq. (2). Here, \dot{W}_1 and \dot{W}_2 are the power calculated based on the given isentropic efficiencies. The efficiency of the electric motors was accounted for by the electric efficiency, η_e .

$$COP = \frac{\dot{Q}_5 + \dot{Q}_3}{\dot{W}_1 + \dot{W}_2} \eta_e \tag{2}$$

The displacement volume of the compressor was found by:

$$\dot{V}_{dis} = \frac{\dot{V}_2}{\eta_{vol,1}} \tag{3}$$

Here, \dot{V}_2 is the suction line volume flow rate, calculated by the mass flow rate and specific volume of stream 2:

$$\dot{V}_2 = v_2 \dot{m}_2 \tag{4}$$

Further, $\eta_{vol,1}$ is the volumetric efficiency of the compressor.

A constant compressor and pump isentropic efficiency of, $\eta_{is} = 0.8$, was used. The electrical efficiency of the electric motors driving the pump and compressor was $\eta_e = 0.95$. The compressor volumetric efficiency was $\eta_{vol} = 0.90$.

It was ensured that the system components were within the technological limitation of commercial components. High pressure ammonia components are available up to a working pressure of 50 bar [4].

Further, the compressor discharge temperature should be limited to ensure the thermal stability of the lubricant. Neksa et al. [27] state that using synthetic oil should allow discharge temperatures up to 180 °C. It was an assumption in the present study that temperatures up to 200 °C were feasible.

Heat transfer and pressure drop modelling

All heat exchangers were assumed to be of a plate type with a chevron corrugation. The working principle of a plate heat exchanger is depicted in Fig. 3. As seen, a counter current arrangement was applied. The plate design may be seen in Fig. 4 and the plate dimensions are listed in Table 1. A smaller plate size was applied for the IHEx and

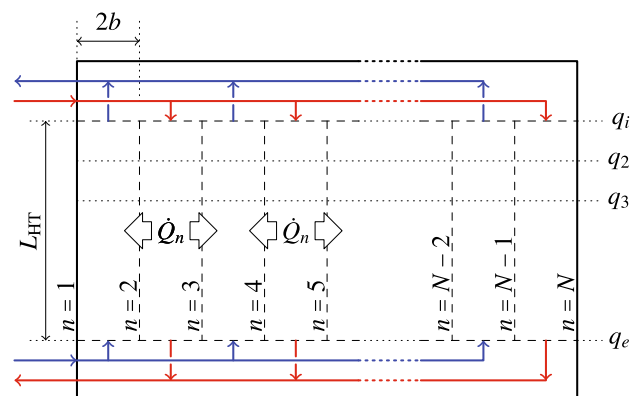


Fig. 3 Principle sketch of the plate heat exchanger

gas-cooler, due to the large difference in mass flow rate between the two streams. This will lead to a large pressure drop if the plate size is not reduced. Reducing the plate size increases the needed number of plates and thus, the cross-sectional area hence, reducing the flow velocity and, consequently, pressure drop.

For the IHEx and gas-cooler, the logarithmic mean temperature difference (LMTD) was applied [18]. For the absorber and desorber, the LMTD was not directly

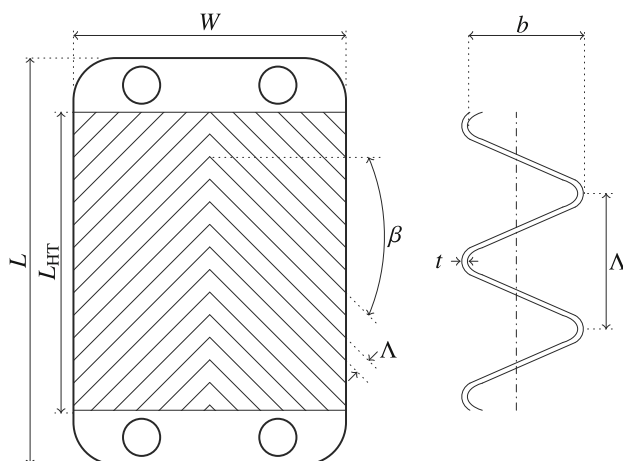


Fig. 4 Plate dimension for chevron corrugated plates

Table 1 Plate dimension for absorber, desorber, gas-cooler and IHEx

	Absorber and desorber	IHEx and gas-cooler
L_p (mm)	525	263
L_{HT} (mm)	456	228
W (mm)	243	122
β (°)	60	60
Λ (mm)	9.6	9.6
b (mm)	2.5	2.5
t (mm)	0.4	0.4
λ_p (W/mK)	14.06	14.06

applicable, as enthalpy and temperature are not proportional [21]. Therefore, the LMTD was determined for each of the thirty steps of the absorber and desorber discretization. An average of the thirty values was applied to determine the heat transfer area. The overall heat transfer coefficient was found as the inverse of the sum of the average convective resistance of the hot and cold side and the conductive resistance in the material separating the two streams.

Palm and Claesson [28] reviewed several single- and two-phase heat transfer correlations for plate exchangers and suggested that Martin's [29] is to be used. This is a semi-empirical correlation based on a heat transfer to friction analogy. Taboás et al. [30–32] investigate the two-phase flow of ammonia–water mixtures in plate heat exchanger during desorption. This work resulted in a correlation, which was applied in the present study.

No correlation directly addresses the two-phase flow of ammonia–water under absorption. Nordtvedt [33] suggested the use of the Silver [34], Bell and Ghaly [35] method. Here, the two-phase heat transfer coefficient was calculated based on: the heat transfer coefficient of the vapour phase, the heat transfer coefficient of the liquid film (corrected for two-phase flow effects) and the gradient of the equilibrium absorption curve.

A list of applied heat transfer and pressure drop correlations are stated in Table 2, here, it is also indicated to which streams they were applied. Both heat transfer coefficient and friction factor, of the two-phase flows in the absorber and desorber, depend on the vapour quality, q . Therefore, an average of heat transfer coefficient and friction factor was determined based on a discretization in q . Twenty steps were applied.

Exergy analysis

To derive the exergy destruction in all components, the specific exergy of all streams was found. The specific

Table 2 Applied heat transfer and pressure drop correlations for the absorber, desorber, gas-cooler and IHEx

k th	Component	j th stream	Media		Heat transfer	Pressure drop
(3)	Gas-cooler	13	H ₂ O		Martin [29]	Martin [29]
(3)	Gas-cooler	3	NH ₃ /H ₂ O		Martin [29]	Martin [29]
(5)	Absorber	12	H ₂ O		Martin [29]	Martin [29]
(5)	Absorber	5	NH ₃ /H ₂ O	Vapour only:	Martin [29]	
				Liquid film:	Yan et al. [36]	
				Two-phase:	Silver [34], Bell and Ghaly [35]	Yan et al. [36]
(6)	IHEx	6 and 11	NH ₃ /H ₂ O		Martin [29]	Martin [29]
(8)	Desorber	15	H ₂ O		Martin [29]	Martin [29]
(8)	Desorber	8	NH ₃ /H ₂ O	Liquid only:	Martin [29]	
				Two-phase:	Táboas et al. [30]	Táboas et al. [30]



exergy is the sum of two contributions: a physical part e^{PH} , associated with reaching thermal and mechanical equilibrium with the dead state, and a chemical part e^{CH} , associated with reaching chemical equilibrium with the dead state [37]. The definition of physical exergy is given by Eq. (5) [18]. Here, $h_{j,0}$ and $s_{j,0}$ are the specific enthalpy and entropy evaluated at the dead-state temperature and pressure and the chemical composition of the j th stream. The dead state in this study was chosen at $T_0 = 25\text{ }^\circ\text{C}$ and $p_0 = 1.013$ bar.

$$e_j^{PH} = h_j - h_{j,0} - T_0(s_j - s_{j,0}) \tag{5}$$

The specific chemical exergy of the ammonia–water mixture was calculated using Eq. (6) [18, 38]. Here, $e_{NH_3}^{CH}$ and $e_{H_2O}^{CH}$ are the standard molar chemical exergy of ammonia and water, respectively. At a temperature of $25\text{ }^\circ\text{C}$ and pressure of 1.013 bar, these attain values of: $e_{NH_3}^{CH} = 336,684\text{ kJ/kmol}$ and $e_{H_2O}^{CH} = 45\text{ kJ/kmol}$ [18]. Further, $w_{X_j}^{rev}$ is the reversible specific work associated with the mixing of pure ammonia and pure water [38]. One value of specific chemical exergy was calculated for each of the three concentrations in the system, x_r , x_l and x_v .

$$e_j^{CH} = x_j e_{NH_3}^{CH} + (1 - x_j) e_{H_2O}^{CH} + w_{X_j}^{rev} \tag{6}$$

$$w_{X_j}^{rev} = (h_{j,0} - x_j h_{NH_3,0} - (1 - x_j) h_{H_2O,0}) - T_0(s_{j,0} - x_j s_{NH_3} - (1 - x_j) s_{H_2O,0}) \tag{7}$$

When the specific exergy of all streams was calculated the total exergy flow rate associated with each stream was determined as the product of the specific exergy of the j th stream and the stream mass flow rate:

$$\dot{E}_j = \dot{m}_j (e_j^{PH} + e_j^{CH}). \tag{8}$$

The control volumes surrounding the compressor and pump were assumed to be adiabatic and, therefore, exchange only mass and work. The remaining components were assumed to be surrounded by an adiabatic and zero-work boundary and thus, all transferred exergy was related to the transfer of material streams. For components in which an exergetic

fuel and product can be defined, the exergy destruction was found as the difference between these:

$$\dot{E}_{D,k} = \dot{E}_{F,k} - \dot{E}_{P,k} \tag{9}$$

For these components, the product and fuel definitions may be seen in Table 3.

Components such as the mixer and the throttling valve are dissipative components. Therefore, a meaningful exergetic fuel and product cannot be defined [18]. For these components, the exergy destruction was found by applying an exergy balance to the component control volume:

$$\dot{E}_{D,4} = \dot{E}_4 + \dot{E}_{11} - \dot{E}_5 \tag{10}$$

$$\dot{E}_{D,7} = \dot{E}_7 - \dot{E}_8 \tag{11}$$

To evaluate the exergetic performance of the components, an exergy efficiency, ε_k , was defined, Eq. (12) [18]. Further, two exergy destruction ratios were used: y_k and y_k^* , Eqs. (13) and (14) [18]. Here, y_k is the exergy destruction in the k th component relative to the total exergy fuel supplied to the system. While, y_k^* is the exergy destruction in the k th component relative to the total exergy destruction in the system.

$$\varepsilon_k = \frac{\dot{E}_{P,k}}{\dot{E}_{F,k}} \tag{12}$$

$$y_k = \frac{\dot{E}_{D,k}}{\dot{E}_{F,tot}} \tag{13}$$

$$y_k^* = \frac{\dot{E}_{D,k}}{\dot{E}_{D,tot}} \tag{14}$$

Exergoeconomic analysis and optimization

Exergoeconomic analysis and optimization is a method for estimating and minimizing the total cost of a single component or an energy conversion system as a whole, over the course of its lifetime [18]. The objective of an exergoeconomic optimization is the minimization of the component or system product cost rate, \dot{C}_P .

Table 3 Definition of exergy fuel and product and fuel and product cost

k th	Component	$\dot{E}_{F,k} =$	$\dot{E}_{P,k} =$	$\dot{C}_{F,k} =$	$\dot{C}_{P,k} =$	Auxiliary relation
(1)	Compressor	\dot{W}_1	$\dot{E}_3 - \dot{E}_2$	$c_w \dot{W}_1$	$\dot{C}_3 - \dot{C}_2$	
(2)	Pump	\dot{W}_2	$\dot{E}_{10} - \dot{E}_9$	$c_w \dot{W}_2$	$\dot{C}_{10} - \dot{C}_9$	
(3)	Gas-cooler	$\dot{E}_3 - \dot{E}_4$	$\dot{E}_{14} - \dot{E}_{13}$	$\dot{C}_3 - \dot{C}_4$	$\dot{C}_{14} - \dot{C}_{13}$	$c_3 = c_4$
(5)	Absorber	$\dot{E}_5 - \dot{E}_6$	$\dot{E}_{13} - \dot{E}_{12}$	$\dot{C}_5 - \dot{C}_6$	$\dot{C}_{13} - \dot{C}_{12}$	$c_5 = c_6$
(6)	IHEX	$\dot{E}_6 - \dot{E}_7$	$\dot{E}_{11} - \dot{E}_{10}$	$\dot{C}_6 - \dot{C}_7$	$\dot{C}_{11} - \dot{C}_{10}$	$c_6 = c_7$
(8)	Desorber	$\dot{E}_{15} - \dot{E}_{16}$	$\dot{E}_1 - \dot{E}_8$	$\dot{C}_{15} - \dot{C}_{16}$	$\dot{C}_1 - \dot{C}_8$	$c_{15} = c_{16}$
System		$\dot{E}_{F,1} + \dot{E}_{F,2} + \dot{E}_{F,8}$	$\dot{E}_{P,3} + \dot{E}_{P,5}$	$\dot{C}_{F,1} + \dot{C}_{F,2} + \dot{C}_{F,8}$	$\dot{C}_{P,3} + \dot{C}_{P,5}$	

By the application of a cost balance [18], the product cost rate for a single component can be derived as:

$$\dot{C}_{P,k} = \dot{Z}_k + \dot{C}_{F,k} \tag{15}$$

Utilizing that: $\dot{E}_D = \dot{E}_F - \dot{E}_P$ and $\dot{C}_D = c_F \dot{E}_D$, this becomes:

$$\dot{C}_{P,k} = \underbrace{\dot{Z}_k}_{\text{Investment}} + \underbrace{\dot{C}_{D,k} + c_{F,k} \dot{E}_{P,k}}_{\text{Operation}} \tag{16}$$

Equally for the system as a whole:

$$\dot{C}_{P,\text{sys}} = \underbrace{\sum_{k=1}^K \dot{Z}_k}_{\text{Investment}} + \underbrace{\dot{C}_{D,\text{sys}} + c_{F,\text{sys}} \dot{E}_{P,\text{sys}}}_{\text{Operation}} \tag{17}$$

As seen in Eqs. (16) or (17), the cost of the component or system product is comprised of three contributions, 1: the capital investment cost rate \dot{Z} , 2: the exergy destruction cost rate \dot{C}_D and 3: the term $c_F \dot{E}_P$. As indicated in Eqs. (16) and (17), the sum of \dot{C}_D and $c_F \dot{E}_P$ can be viewed as the operational cost of the component or system and will in the following be referred to as:

$$\dot{C}^{\text{OP}} = \dot{C}_D + c_F \dot{E}_P \tag{18}$$

In the current study, the objective is the minimization of the cost of heat supplied by the HACHP and is thus a minimization of $\dot{C}_{P,\text{sys}}$, the definition of which is stated in Table 3. The objective for the HACHP system can be stated as:

$$\text{Objective function: } \min \left(\sum_{k=1}^K \dot{Z}_k + \dot{C}_{\text{sys}}^{\text{OP}} \right) \tag{19}$$

The objective of the optimization is thus to balance the cost of capital investment with the cost of operation. From Eq. (18), it is clear that the cost of operation can be

reduced by increasing exergy efficiency and consequently reducing the cost of exergy destruction, $\dot{C}_{D,\text{sys}}$. However, for most components, this will require an increased investment, e.g. for a heat exchanger, the exergy efficiency is increased if the temperature difference is reduced, consequently the heat transfer area and subsequently the investment must increase to adapt to the reduced temperature difference.

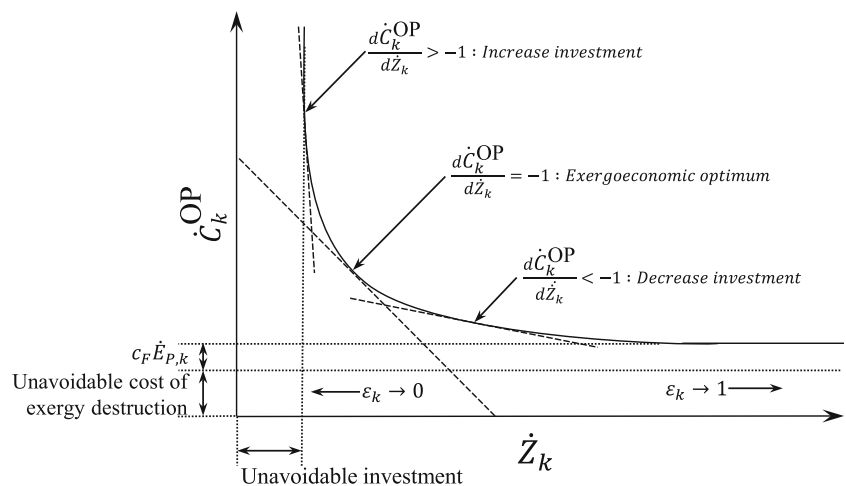
This behaviour is depicted in Fig. 5. Here, it may be seen that the relation of \dot{C}_k^{OP} to \dot{Z}_k has a horizontal and vertical asymptote. As the investment approaches infinity, some exergy destruction will prevail, due to technological limitations, this is known as the unavoidable exergy destruction [39]. Further, no matter how much the exergy efficiency is decreased, some investment will be needed, this is known as the unavoidable investment [39]. This behaviour is limiting for system improvement based on the conventional exergoeconomic analysis as this uses indicators based on absolute values of \dot{C}_D and \dot{Z} and thus does not account for the unavoidable parts.

In the present study, cost functions for the component product equipment cost (PEC) were applied. Therefore, component investment costs were expressed mathematically, as a function of the HACHP design. This also allows the exergoeconomic optimum to be defined mathematically.

As seen in Fig. 5, the exergoeconomic optimum choice of exergy efficiency, ϵ_k , is defined where the marginal cost rate of the levelized investment and maintenance cost, \dot{Z}_k , is equal to the marginal cost rate of operation, \dot{C}_k^{OP} . Mathematically, this statement can be justified by taking the derivative of Eq. (16) with respect to the exergy efficiency, ϵ_k :

$$\frac{d\dot{C}_{P,k}}{d\epsilon_k} = \frac{d\dot{Z}_k}{d\epsilon_k} + \frac{d\dot{C}_k^{\text{OP}}}{d\epsilon_k} \tag{20}$$

Fig. 5 Graphical representation of the exergoeconomic optimum



Thus, if $\frac{d\dot{Z}_k}{d\epsilon_k} = -\frac{d\dot{C}_k^{OP}}{d\epsilon_k}$ then $\frac{d\dot{C}_{P,k}}{d\epsilon_k} = 0$ and it can be confirmed that an optimum condition is attained. Further, if the component follows the behaviour seen in Fig. 5, this optimum will be the global minimum for $\dot{C}_{P,k}$ as: $\dot{C}_{P,k} \rightarrow \infty$ for both $\epsilon_k \rightarrow 0$ and $\epsilon_k \rightarrow 1$

Hence, for a component that follows the behaviour seen in Fig. 5, the cost of the component exergy product, Eq. (16), is minimized when:

$$\frac{d\dot{C}_k^{OP}}{d\dot{Z}_k} = -1 \tag{21}$$

Subsequently, if:

$$\frac{d\dot{C}_k^{OP}}{d\dot{Z}_k} > -1 \tag{22}$$

the total cost can be reduced by increasing the exergy efficiency, at the expense of an increased investment. Conversely, if:

$$\frac{d\dot{C}_k^{OP}}{d\dot{Z}_k} < -1 \tag{23}$$

the total cost is reduced by reducing the investment, at the expense of a reduced exergy efficiency.

The design of the HACHP was governed by four decision variables. These were, $\Delta T_{pp,k}$ for the absorber and desorber and ϵ_k for the IHX and gas-cooler. A change in these variables will all exhibit the behaviour presented in Fig. 5. It was the objective of the exergoeconomic optimization to determine the optimum values of these four variables. This was done by an iterative optimization procedure minimizing the objective function stated in Eq. (19).

Initial guess values for the four decision variables were made. Using the ‘‘Uncertainty Propagation’’ procedure in EES [23], the partial derivatives of both the investment cost rate, \dot{Z}^Σ and the operational cost rate, \dot{C}_{sys}^{OP} , were found with respect to the four decision variables individually. The superscript Σ , here indicates the sum over all K components. Based on these partial derivatives, it was decided whether to increase or decrease the values. E.g. if:

$$\left| \frac{\partial \dot{C}_{sys}^{OP}}{\partial \Delta T_{pp,5}} \right| > \left| \frac{\partial \dot{Z}^\Sigma}{\partial \Delta T_{pp,5}} \right| \tag{24}$$

the absorber pinch-point temperature difference should be reduced.

This procedure was repeated until:

$$\left(\frac{\partial \dot{C}_{sys}^{OP}}{\partial \dot{Z}^\Sigma} \right)_k \in \{-0.9, -1.1\} \tag{25}$$

for all the four decision variables simultaneously, at which an optimum was said to be attained.

To justify this approach, the results of the described procedure will, for one case, be compared to the result of a Genetic Optimization Algorithm maximizing the present value of the savings attained by the installation. The boundaries for the decision variables were set to: $\Delta T_{pp} \in \{1; 20\}$ and $\epsilon \in \{0; 1\}$. The Genetic Optimization Algorithm was performed with 32 individuals and 64 generations. The build in Genetic Optimization Algorithm in EES [23] was applied.

The yearly savings in operational costs attained by the installations was determined as:

$$\text{Savings}_{\text{yearly}} = \dot{Q}_{HP} h_{op} \left(c_{\text{gas}} - \frac{c_{\text{elec}}}{\text{COP}} \right) \tag{26}$$

Here, c_{gas} and c_{elec} are the gas and electricity prices, respectively, and h_{op} is the operating time per year. The present value of the savings, including the initial capital investment and maintenance cost, over the technical lifetime was then calculated as:

$$\text{Savings} = \frac{\text{Savings}_{\text{yearly}}}{\text{CRF}} - 1.2 \cdot \text{Investment} \tag{27}$$

Here, CRF is the Capital Recovery Factor as given in [18], calculated based on the interest rate, inflation rate and technical lifetime stated in section ‘‘Component investment cost and levelization’’. The factor of 1.2 accounts for the component maintenance cost as also discussed in section ‘‘Component investment cost and levelization’’.

To conduct this optimization, the exergy cost rate, \dot{C}_j , of all streams was determined. This was done by applying cost balances to all components. A number of auxiliary relations were needed, these were determined based on the F-rule [18] and are listed in Table 3. Further, it was assumed that the specific unit cost of exergy for the vapour stream and liquid stream exiting the separator were equal: $c_2 = c_9$ and that no cost was affiliated with the inlet condition of the sink and source: $c_{12} = c_{15} = 0$ €/s.

The definitions of the fuel and product costs, for the non-dissipative components and for the total HACHP system, are stated in Table 3. Using these definitions, the component-specific fuel, $c_{F,k}$ and product, $c_{P,k}$ costs were determined, Eqs. (28) and (29).

$$c_{F,k} = \frac{\dot{C}_{F,k}}{\dot{E}_{F,k}} \tag{28}$$

$$c_{P,k} = \frac{\dot{C}_{P,k}}{\dot{E}_{P,k}} \tag{29}$$

Further, the conventional exergoeconomic indicators were determined. These were the exergoeconomic factor, f_{ex} see Eq. (30), indicating the impact of the non-exergetic cost on the total cost and the relative cost difference, r see Eq. (31), indicating the relative increase in cost between the fuel and product of a component.

$$f_{ex,k} = \frac{\dot{Z}_k}{\dot{Z}_k + c_{F,k}\dot{E}_{D,k}} \quad (30)$$

$$r_k = \frac{c_{P,k} - c_{F,k}}{c_{F,k}} \quad (31)$$

Component investment cost and levelization

PEC cost functions were developed based on Danish intermediate trade business prices [40, 41] and individual producers [42]. Prices correspond to the year 2012. The cost functions were constructed as proposed by Bejan et al. [18]. A number of assumptions have been made to estimate the total investment of the HACHP system. These were as follows:

- Total capital investment of a component was 4.16 higher than the PEC of the component [18].
- PEC for a compressor was a function of the compressor displacement volume.
- PEC for an electrical motor with a fixed efficiency was dependent only on the shaft power.
- PEC for a heat exchanger was a function of the heat exchange area.
- PEC of the pump was equivalent to its electrical motor.
- PEC of the expansion valve, mixer and the liquid–vapour separator was neglected.

To determine the levelized capital component cost rates, the capital recover factor [18] was applied. An interest rate of 7 % and inflation rate of 3 % were assumed. Further, the technical lifetime was 15 years with 3000 operating hours per year. The component maintenance cost rate was assumed to be 20 % of the levelized capital cost rates. The total investment and maintenance cost rate (non-exergetic cost rate), \dot{Z} , was the sum of the levelized capital investment and maintenance cost rate.

Electricity and natural gas prices correspond to an industrial process consumer in the Danish fiscal environment, prices were found in [2] and correspond to the year 2012.

Results

Thermodynamic analysis

The ammonia mass fraction of the rich solution and the circulation ratio both have great influence on both the COP and the pressure levels in the system. As described by Jensen et al. [5] and Zamjirescu [43], it is important to find the correct combination of these two parameters. Figure 6 shows the COP of the HACHP, as a function of the ammonia mass fraction and circulation ratio, with $\Delta T_{pp,5} =$

$\Delta T_{pp,8} = 10$ K and $\epsilon_3 = \epsilon_6 = 0.7$. Figure 6a is for a HACHP covering 10 % of the total heat load. Figure 6b is for 15 %, Fig. 6c for 20 % and Fig. 6d is for 25 %. The solutions with $x_r < 0.55$ are discarded, as these tend to result in sub-atmospheric desorber pressures and large volumetric flow rates in the compressor suction line [5]. It is seen, that for all four load shares, in the range of $x_r > 0.55$, one circulation ratio optimizes the COP for each value of x_r . The optimum COP line for all four loads is shown with the dashed line. It can be seen that this line shifts downwards as the HACHP load is increased. Hence, the higher the load, the lower the circulation ratio. This is mainly due to the increased temperature glide in the heat sink.

Four points are chosen at each HACHP load, these are with x_r of: 0.6, 0.7, 0.8 and 0.9 and the corresponding optimum circulation ratios. These points are indicated with circles on Fig. 6.

Exergoeconomic optimization

The exergoeconomic analysis can then be applied to determine the exergoeconomic optimum design, at the 16 points derived from the thermodynamic analysis. Table 4 shows the result of the exergoeconomic analysis, at an initial set of guess values and at the exergoeconomic optimum. Both have a HACHP load of 15 % and a rich ammonia mass fraction $x_r = 0.8$. The initial guess values are $\Delta T_{pp,5} = \Delta T_{pp,8} = 15$ K and $\epsilon_3 = \epsilon_6 = 0.9$.

As may be seen in Table 4, for the initial guess values, the total cost rate for the gas-cooler is the third highest only surpassed by the compressor and absorber. The gas-cooler also has the second highest relative cost difference. Judging from the low exergoeconomic factor, conventional exergoeconomic optimization states that the investment should be increased, but judging from the partial derivative the investment should actually be decreased to reduce the overall cost.

This difference arises, as the partial derivatives account for both the interdependencies between component exergy efficiencies and for the unavoidable part of exergy destruction and investment.

In the case of the absorber and IHX, it may be seen that the conclusions of the conventional exergoeconomic analysis and the partial derivatives coincide.

The exergoeconomic factor for the desorber is $f_{ex,8} = 1$. This is because no cost is associated with the waste heat and thus, $c_{F,k} = 0$. Therefore, the relative cost difference cannot be calculated as, $c_{F,k}$ is the fraction denominator. This makes it hard to judge whether or not the choice of the design parameter for the desorber is appropriate. However, judging from the partial derivative, it is clear that savings to the overall cost can be attained by increasing the desorber exergy efficiency.

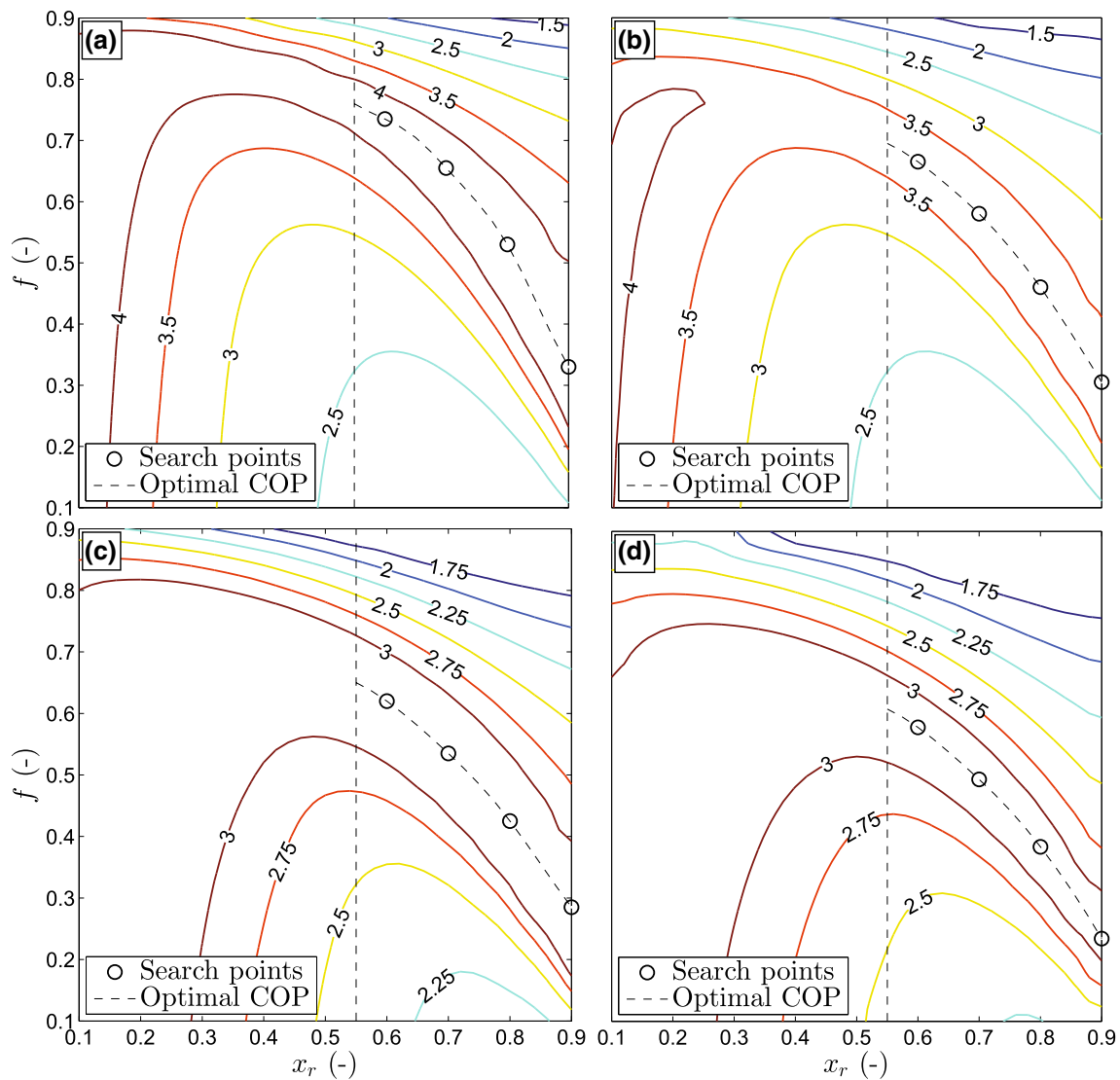


Fig. 6 COP of the HACHP as function of x_r and f for a HACHP covering **a** 10 %, **b** 15 %, **c** 20 % and **d** 25 % of the total heat load

The conclusion from the partial derivatives of the initial guess is that: The effectiveness of the IHEX and gas-cooler should be reduced to lower the investment, the IHEX effectiveness should be lowered more than for the gas-cooler. Further, the absorber and desorber pinch-point temperature difference should both be reduced, more for the desorber than for the absorber.

Table 4 states the cost rates and exergoeconomic indicators at the optimum values of the decision variables, suggested by the partial derivatives. Here, the absorber and desorber pinch-point temperature differences are reduced to $\Delta T_{pp,5} = 11.3$ K and $\Delta T_{pp,8} = 9.49$ K, respectively. The IHEX effectiveness is reduced to $\epsilon_6 = 0.719$ and the gas-cooler effectiveness to $\epsilon_3 = 0.864$. Hence, the direction and the magnitude of the change in variables are consistent with the conclusion of the partial derivatives from the initial guess. Further, it can be seen that only the

exergoeconomic factor and relative cost difference of the IHEX undergo substantial change between the initial guess and the optimum.

The present value of the savings attained by the HACHP is 81,138 € with the initial guess values. This is increased by 70 %, at the exergoeconomic optimum, to a value of 138,078 €. The physical variables of the HACHP process, for the exergoeconomic optimum from Table 4, are listed in Table 5.

Further, the results of a Genetic Optimization Algorithm maximizing the present value of the savings are presented. The Genetic Optimization Algorithm was given the same initial guess as provided to the exergoeconomic optimization. As seen from Table 4, the Genetic Optimization Algorithm finds the same decision variables as found by the exergoeconomic optimization, which suggests that the applied optimization procedure is capable of determining the

Table 4 Non-exergetic and exergetic cost rates and exergoeconomic indicators for the initial guess and optimal solution for a HACHP with $x_r = 0.8$ covering 15 % of the total heat load

k th	Decision var.	$\dot{Z}_k + \dot{C}_{D,k}$ (cent/h)	$f_{ex,k}$ (%)	r_k (%)	$\left(\frac{\partial \dot{C}^{OP}}{\partial \dot{Z}^k}\right)_k$
Initial guess variables					
(1)		779	56	45	–
(2)		16.7	53	60	–
(3)	$\epsilon = 0.9$ –	351	8.3	62	–0.294
(4)	$\Delta T_{pp} = 15$ K	374	26	24	–2.02
(6)	$\epsilon = 0.9$ –	206	75	92	–0.263
(8)	$\Delta T_{pp} = 15$ K	74.8	100	–	–3.64
Objective function value, Eq. (19):			2896 cent/h		
Present value of Savings, Eq. (27):			81,138 €		
Exergoeconomic optimum by partial derivatives					
(1)		728	57	48	–
(2)		15.7	54	61	–
(3)	$\epsilon = 0.864$ –	271	9.6	58	–0.933
(4)	$\Delta T_{pp} = 11.3$ K	387	44	26	–1.00
(6)	$\epsilon = 0.719$ –	76.6	53	54	–1.05
(8)	$\Delta T_{pp} = 9.49$ K	193	100	–	–1.02
Objective function value, Eq. (19)			2742 cent/h		
Present value of Savings, Eq. (27):			138,078 €		
Genetic optimization algorithm maximizing savings					
(1)		728	57	48	–
(2)		15.7	54	61	–
(3)	$\epsilon = 0.864$ –	271	9.6	58	–0.965
(4)	$\Delta T_{pp} = 11.3$ K	387	44	26	–1.04
(6)	$\epsilon = 0.719$ –	76.6	53	54	–1.01
(8)	$\Delta T_{pp} = 9.49$ K	193	100	–	–0.979
Objective function value, Eq. (19):			2742 cent/h		
Present value of Savings, Eq. (27):			138,117 €		

Table 5 Thermodynamic state point variables for the exergoeconomic optimum seen in Table 4, $x_r = 0.8$ and 15 % of the total heat load covered by HACHP

j th	\dot{m}_j (kg/s)	p_j (bar)	T_j (°C)	x_j (–)	h_j (kJ/kg)	s_j (kJ/kgK)	$v_j \cdot 10^{-3}$ (m ³ /kg)	e^{PH} (kJ/kg)	e^{CH} (kJ/kg)
1	1.387	13.32	64.25	0.8000	776.4	2.802	61.10	220.6	15,875
2	0.7490	13.32	64.25	0.9947	1386	4.518	112.0	360.0	19,764
3	0.7490	49.10	196.6	0.9947	1665	4.638	41.99	603.2	19,764
4	0.7490	49.10	125.6	0.9947	1428	4.106	31.77	524.5	19,764
5	1.3870	49.10	119.5	0.8000	857.6	2.753	15.27	316.4	15,875
6	1.3870	49.10	100.6	0.8000	354.9	1.433	1.712	207.2	15,875
7	1.3870	49.10	90.09	0.8000	298.7	1.28	1.662	196.6	15,875
8	1.3870	13.32	45.37	0.8000	298.7	1.343	21.61	177.8	15,875
9	0.638	13.32	64.26	0.5714	60.57	0.7866	1.394	56.27	11,311.4
10	0.638	49.10	65.27	0.5714	66.48	0.7901	1.319	61.12	11,311.4
11	0.638	49.10	90.91	0.5714	188.5	1.138	1.385	79.55	11,311.4
12	7.889	5.000	85.00	–	356.3	1.134	–	23.00	–
13	7.889	4.971	106.0	–	444.7	1.374	–	40.00	–
14	7.889	4.674	111.3	–	467.2	1.433	–	45.00	–
15	7.889	5.000	75.00	–	314.3	1.015	–	16.00	–
16	7.889	4.978	54.93	–	230.4	0.7668	–	6.000	–

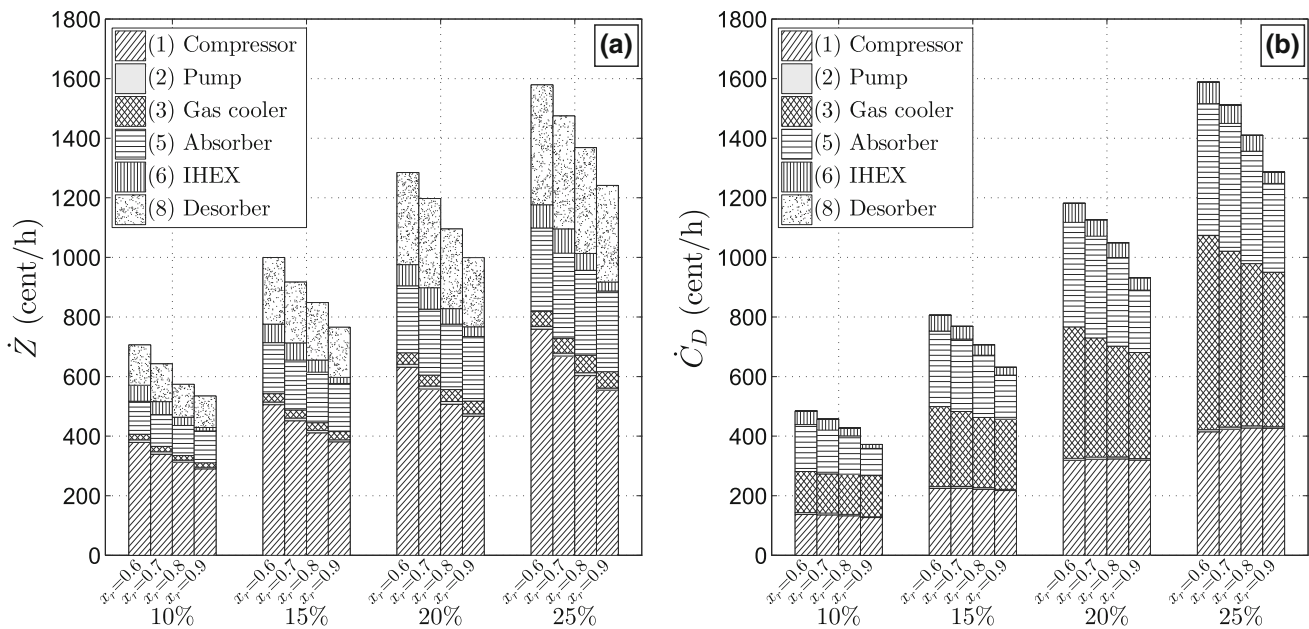


Fig. 7 \dot{Z}_k (a) and $\dot{C}_{D,k}$ (b) of the k th component at HPLs of 10, 15, 20 and 25 % and x_r of 0.6, 0.7, 0.8 and 0.9

true optimum. It is seen that the Genetic Optimization Algorithm finds a savings that is 0.3 % higher than what is attained by the exergoeconomic optimization. However, the partial derivatives also suggest that the solution found by the Genetic Optimization Algorithm is closer to the exergoeconomic optimum. The exergoeconomic approach using partial derivatives found the four optimum decision variables after five iterations, each with a computation time of approximately 1 min. While the computation time for the Genetic Optimization Algorithm was several hours.

This optimization procedure has been conducted for all of the 16 design configurations. Figure 7a shows the non-exergetic cost rate, \dot{Z}_k , for the components at all 16 optimal designs. Figure 7b shows the exergy destruction cost, $\dot{C}_{D,k}$. It may be seen that the total non-exergetic cost rate, \dot{Z}^Σ , increases when decreasing the ammonia mass fraction. This is caused by an increase in the compressor, IHEX and desorber \dot{Z}_k . The remaining components are indifferent to the change in ammonia mass fraction. The compressor \dot{Z}_k increases the most. This is caused by the reduced vapour pressure of the working fluid, resulting in an increased displacement volume. The IHEX \dot{Z}_k is increased due to the increased circulation ratio for reduced ammonia mass fractions. Thereby, the capacity rates of the rich and lean mixtures approach each other, consequently reducing the LMTD and increasing the needed heat load. Both resulting in the need for an increased area. Figure 7a also shows that the total non-exergetic cost rate, \dot{Z}^Σ increases when the heat pump load is increased. The marginal \dot{Z}^Σ is close to constant.

From Fig. 7b, it is seen that the total exergy destruction cost, \dot{C}_D^Σ , increases when decreasing the ammonia mass fraction. It is seen that the cost of operating the compressor is not significantly influenced by the ammonia mass fraction. Further, the gas-cooler $\dot{C}_{D,k}$, is indifferent to x_r for HACHP loads of 10 and 15 %. For the absorber and IHEX, the $\dot{C}_{D,k}$ is increased, when decreasing the ammonia mass fraction. For the absorber, this is caused by the degradation of the two-phase heat transfer coefficient. The reduced heat transfer coefficient shifts the optimal size of the absorber to a lower exergy efficiency. For the IHEX, the increased $\dot{C}_{D,k}$ is caused by the increased circulation ratio. For the desorber, $\dot{C}_{D,k}$ decreases when the ammonia mass fraction is reduced. This, in spite of the decreased heat transfer coefficient. This is caused by the interdependency between the low pressure and the compressor investment, as a larger desorber investment can reduce the compressor investment by increasing the suction line pressure. The total exergy destruction cost, \dot{C}_D^Σ , increases with the delivered heat load. The marginal \dot{C}_D^Σ is also increased with the heat load.

HACHP implementation, economic and environmental savings

Several issues govern the implementation of the HACHP. As shown in Fig. 7, both the choice of ammonia mass fraction and heat pump load influence the investment and the operating costs of the HACHP.

To estimate yearly CO₂ emissions, the fuel-specific emission factors for electricity and natural gas in the Danish energy system are used [2].

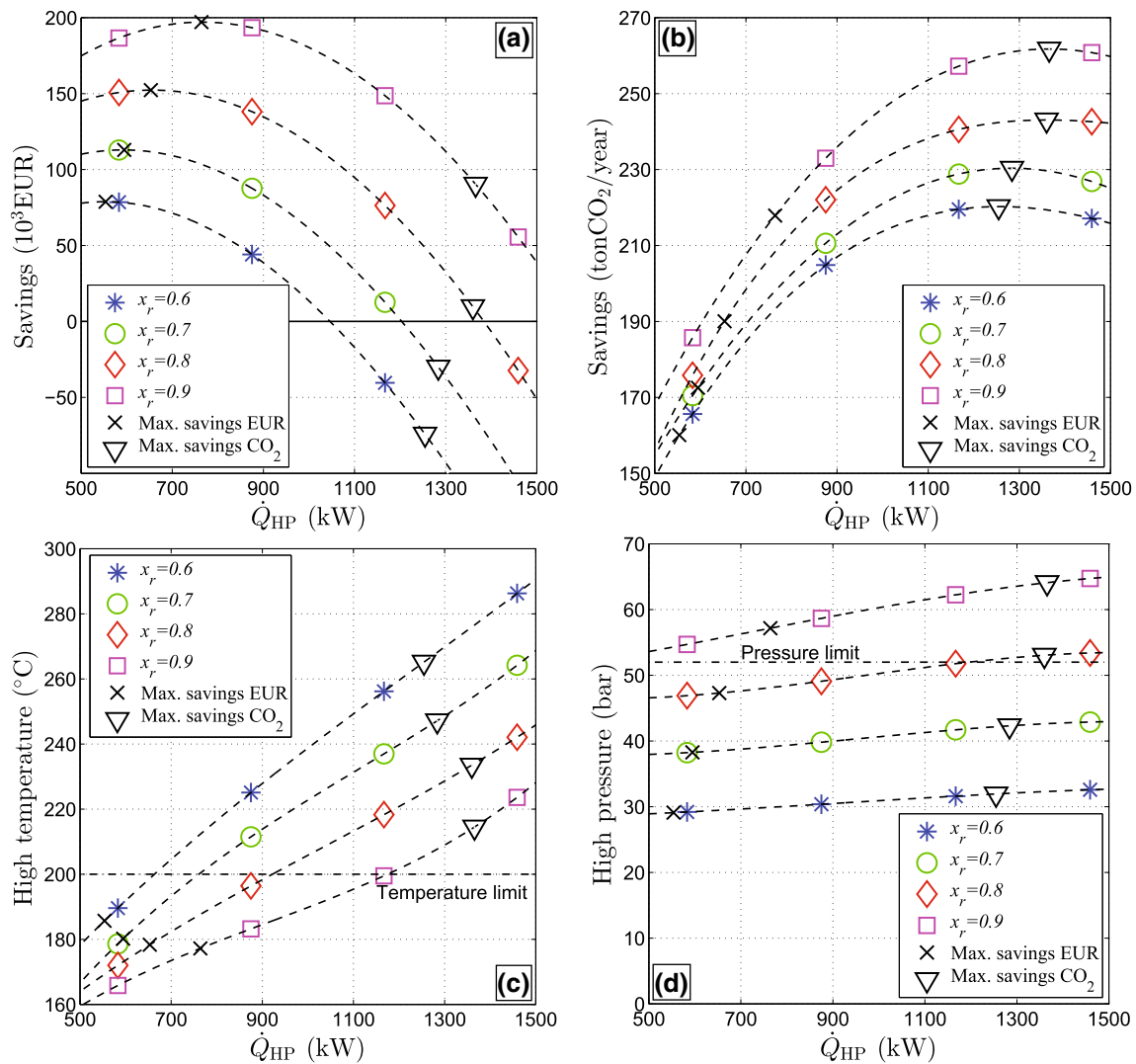


Fig. 8 a Present value of the economic savings. b Yearly CO₂ emission savings. c Compressor discharge temperature. d Compressor discharge pressure. All shown a function of the design heat pump load and ammonia mass fraction

Figure 8 shows the economic and CO₂ savings as well as the compressor discharge temperature and pressure. All are shown as a function of the HACHP load \dot{Q}_{HP} . The values are given for the exergoeconomic optimum designs. Figure 8a shows the present value of the economic savings in Euro. As can be seen: for each ammonia mass fraction, one heat pump load maximizes the savings. At this point, the marginal total cost of the HACHP (sum of investment and operation) is equal to the marginal cost of gas heating. As seen, the higher the ammonia mass fraction, the higher the savings and the higher the optimum HACHP load. Figure 8b shows the yearly CO₂ emissions savings. It can be seen that the maximum emission savings occur at a higher HACHP load than the maximum economic savings. Further, it is seen that, the higher the ammonia mass fraction, the higher the emissions savings.

Figure 8c shows the compressor discharge temperature and the temperature limit. It can be seen that none of the economic optimum loads are restricted by the temperature limit, while all of the optimum emission loads exceed this constraint. Further, it can be seen that increasing the ammonia mass fraction decreases the compressor discharge temperature. Figure 8d shows the compressor discharge pressure. Here, it can be seen that only the optimal savings for $x_r = 0.9$ is restricted by the pressure limit. Further, it can be seen that increasing the ammonia mass fraction increases the discharge pressure.

As the best possible implementation of the HACHP may be one with an ammonia mass fraction between the curves shown in Fig. 8, an interpolation between HACHP load and the ammonia mass fraction for the 16 exergoeconomic optimum points has been made.

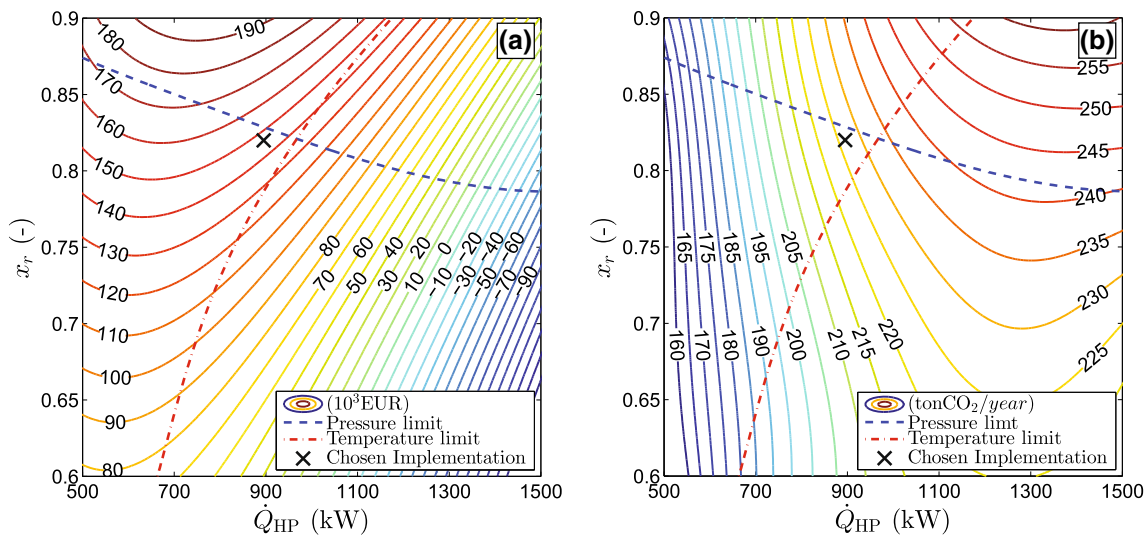


Fig. 9 **a** Interpolation of the economic savings. **b** Interpolation of the emission savings. Both as a function of the design heat load and ammonia mass fraction and with compressor discharge pressure and temperature limit imposed

Table 6 Results of the exergy and exergoeconomic analysis of the chosen implementation

kth	Component	$\dot{E}_{P,k}$ (kW)	$\dot{E}_{F,k}$ (kW)	$\dot{E}_{D,k}$ (kW)	ε_k (%)	y_k (%)	y_k^* (%)	\dot{Z}_k (cent/h)	$\dot{C}_{D,k}$ (cent/h)	$f_{ex,k}$ (%)	r_k (%)
1	Compressor	187	226	38.7	83	13	29	415	322	56	47
2	Pump	2.99	3.82	0.830	78	0.27	0.63	8.35	6.92	55	61
3	Gas-cooler	40.3	61.3	21.0	66	6.8	16	27.6	253	10	58
4	Mixer	–	–	4.95	–	1.6	3.7	27.2	–	–	0
5	Absorber	136	154	18.0	88	5.8	14	172	214	45	26
6	IHEX	11.4	14.3	2.95	79	0.95	2.2	38.8	35.5	52	54
7	Throttling valve	–	–	26.7	–	8.6	20	0	–	–	–
8	Desorber	59.8	79.4	19.6	75	6.3	15	190	0	100	–

Figure 9a shows the interpolation of economic savings with the pressure and temperature limits imposed. The area below the blue-dashed line satisfies the pressure constraint, while the area to the left of the red dash-dot line satisfies the temperature constraint. A similar plot for the emission savings is shown in Fig. 9b. The chosen implementation is indicated by the \times . This is chosen to attain both high economic and emission savings. The chosen load is $\dot{Q}_{HP} = 895$ kW with an ammonia mass fraction 0.82. The circulation ratio is then 0.43. The exergoeconomic optimum values of pinch-point temperature difference and effectiveness are: $\Delta T_{pp,5} = 11.2$ K, $\Delta T_{pp,8} = 8.98$ K, $\varepsilon_6 = 0.730$ and $\varepsilon_3 = 0.864$. Here, the present value of the saving is 146,426 € and the yearly CO₂ emissions are reduced by a total 227 ton.

Table 6 shows the results of the exergy and exergoeconomic analysis of the chosen implementation. As seen, the highest contribution to the exergy destruction in the system is caused by the compressor and the throttling valve, both accounting for 22 % of the total exergy

destruction. The gas-cooler, absorber and desorber are the other main contributors, responsible for 17, 16 and 15 %, respectively. The component with the highest total cost rate is the compressor, while this component has the second lowest relative cost difference. The highest relative cost difference is found in the gas-cooler.

Discussion

In the present study, partial derivatives were applied as an aid to determine the exergoeconomic optimum of the HACHP, which proved to be a helpful tool. However, this approach was only applicable due to the application of cost functions. Thereby, the investment cost of a component was linked mathematically to the choice of the design variables, which allows the numerical partial derivatives to be determined. In real-life applications, this is hardly ever the case, wherefore, the partial derivatives cannot be attained. In these cases, the advanced exergoeconomic

analysis, as applied in [44], could be used. The advanced exergoeconomic method can explicitly determine the unavoidable costs of both investment and operation and component interdependencies and does not require the application of cost function. The advanced exergoeconomic method does not constitute a mathematical optimization procedure, but defines the best possible design as one at which the advanced exergoeconomic factors for all components are 50 %. The advanced exergoeconomic factor is calculated as seen in Eq. (30), but subtracts the unavoidable parts of \dot{Z}_k and $\dot{C}_{D,k}$ shown in Fig. 5. Thus, if the advanced exergoeconomic factor is close to 50 %, it is likely that the design is close to the exergoeconomic optimum.

Further, the use of cost functions would allow the application of any mathematical optimization procedure to maximize the savings, without the use of exergy or exergoeconomics. This approach would, however, not yield the detailed information on the sources of investment and operational cost that is attained with the exergoeconomic analysis.

This information is gathered in Table 6 and from this, insight to how the HACHP can be further improved is attained. As can be seen in Table 6, the gas-cooler accounts for both a significant part of the exergy destruction cost rate and also has the highest relative cost difference. The high cost rate and relative cost difference are caused by the superheat of the gas exiting the compressor. This cannot be changed directly by changing the design of the gas-cooler, but could be reduced by the implementation of a two-stage compression. This could also reduce the exergy destruction cost of the compression. Therefore, this could prove to be a good improvement of the system.

Ommen et al. [12] tested ammonia mass fractions of 0.7 and 0.9 and also found the total cost to increase with the reduction of ammonia mass fraction. The optimum pinch-point temperatures found in [12] are significantly lower than those presented in the current study. This is assumed to be caused by the use of constant overall heat transfer coefficient applied in [12]. Hence, the degradation of two-phase heat transfer due to mass diffusion resistance is not captured. This has been shown to have an influence on both the PEC and the exergoeconomic optimum design and should be accounted for.

Conclusion

The implementation of a HACHP in a spray-drying facility was investigated and optimized. Heat transfer and pressure drop correlations from the open literature were gathered and implemented in the thermodynamic model of the HACHP. Cost functions based on Danish intermediate

trade price were constructed to assess the heat pump investment. The exergoeconomic method has been used to minimize the total cost of the HACHP. The influence of ammonia mass fraction, circulation ratio and heat pump load was also investigated. Constraints based on commercially available technologies were imposed.

The best possible implementation was found to be a 895 kW HACHP with an ammonia mass fraction of 0.82 and circulation ratio of 0.43. This resulted in an economic saving with a present value of 146,426 € and a yearly reduction of the CO₂ emissions by 227 ton.

The use of numerical partial derivatives was applied to implicitly account for the unavoidable costs and component interdependencies. This gave a more precise indication of the exergoeconomic optimum compared to what is attained based only on the exergoeconomic indicators: exergoeconomic factor and relative cost difference. However, the exergoeconomic indicators still gave valuable insight of the sources of investment and the cost of irreversibilities. The indicators gave useful information to the further improvement of the system.

Acknowledgments This research project is financially funded by EUDP (Energy Technology Development and Demonstration). Project title: “Development of ultra-high temperature hybrid heat pump for process application”, Project Number: 64011-0351.

Open Access This article is distributed under the terms of the Creative Commons Attribution License which permits any use, distribution, and reproduction in any medium, provided the original author(s) and the source are credited.

References

1. Baker, C.G.J., McKenzie, K.A.: Energy consumption of industrial spray dryers. *Dry. Technol.: Int. J.* **23**(1–2), 365–386 (2005). doi:[10.1081/DRT-200047665](https://doi.org/10.1081/DRT-200047665)
2. Energy statistics 2012 (Original language Danish: Energistatistik 2012). Danish Energy Agency, ISSN 0906–4699 (2012)
3. Brunin, O., Feidt, M., Hivet, B.: Comparison of the working domains of some compression heat pumps and a compression–absorption heat pump. *Int. J. Refrig.* **20**(5), 308–318 (1997)
4. Ommen, T., Jensen, J.K., Markussen, W.B., Reinholdt, L., Elmegaard, B.: Technical and economic working domains of industrial heat pumps: part 1—vapour compression heat pumps. *Int. J. Refrig.* (submitted)
5. Jensen, J.K., Reinholdt, L., Markussen, W.B., Elmegaard, B.: Investigation of ammonia/water hybrid absorption/compression heat pumps for heat supply temperatures above 100°C. In: International sorption heat pump conference, University of Maryland. Washington DC, March 31–April 2, 2014
6. Osenbrück, A.: Refrigerating or freezing method in absorption machines (Original language German: Verfahren kalteerzeugung bei absorptions-maschinen) (1895)
7. Altenkirch, E.: Vapour compression refrigeration machine with solution circuit. (Original language German: Kompressionskältemaschine mit lözungskreislauf). *Kältetechnik.* **2**(10,11,12), 251–259, 310–315, 279–284 (1950)



8. Lorenz, H.: Contributions to the assessment of cooling machines (Original language German: Beiträge zur Beurteilung von Kühlmaschinen). *Z VDI*. 38, 62–68, 98–103, 124–130 (1894)
9. Prasertsan, S., Saen-saby, P.: Heat pump dryers: research and development needs and opportunities. *Dry. Technol.: Int. J.* **16**(1–2), 251–270 (1998). doi:[10.1080/07373939808917402](https://doi.org/10.1080/07373939808917402)
10. Gungor, A., Erbay, Z., Hepbasli, A.: Exergoeconomic analyses of a gas engine driven heat pump drier and food drying process. *Appl. Energy* **88**(8), 2677–2684 (2011). doi:[10.1016/j.apenergy.2011.02.001](https://doi.org/10.1016/j.apenergy.2011.02.001)
11. Chua, K.J., Chou, S.K., Ho, J.C., Hawlader, M.N.A.: Heat pump drying : recent developments and future trends. *Dry. Technol.: Int. J.* **20**(8), 1579–1610 (2002). doi:[10.1081/DRT-120014053](https://doi.org/10.1081/DRT-120014053)
12. Ommen, T.S., Markussen, C.M., Reinholdt, L., Elmegaard, B.: Thermoeconomic comparison of industrial heat pump. In: ICR 2011, Prague, Czech Republic 21–26 Aug 2011
13. Collier, J.G., Thome, J.R.: *Convective Boiling and Condensation*. Clarendon Press, Oxford (1994)
14. Radermacher, R., Hwang, Y.: *Vapor Compression Heat Pumps with Refrigerant Mixtures*. Mechanical Engineering. Taylor & Francis, London (2005)
15. Satapathy, P.: Exergy analysis of a compression–absorption system for heating and cooling applications. *Int. J. Energy Res.* 1266–1278 (2008) doi:[10.1002/er.1417](https://doi.org/10.1002/er.1417)
16. Hultén, M., Berntsson, T.: The compression/absorption heat pump cycle—conceptual design improvements and comparisons with the compression cycle. *Int. J. Refrig.* **25**, 487–497 (2002)
17. Hultén, M., Berntsson, T.: The compression/absorption cycle— influence of some major parameters on COP and a comparison with the compression cycle. *Int. J. Refrig.* **22**, 91–106 (1999)
18. Bejan, A., Tsatsaronis, G., Moran, M.J.: *Thermal Design and Optimization*. Wiley-Interscience publication, New York (1996)
19. Kotas, T.J.: *The Exergy Method of Thermal Plant Analysis*. Butterworths, London (1985)
20. Kemp, I.C.: Reducing dryer energy use by process integration and pinch analysis. *Dry. Technol.: Int. J.* **23**(9–11), 2089–2104 (2005). doi:[10.1080/07373930500210572](https://doi.org/10.1080/07373930500210572)
21. Itard, L.C.M., Machielsen, C.H.M.: Considerations when modelling compression/resorption heat pumps. *Int. J. Refrig.* **17**(7), 453–460 (1994)
22. Zheng, N., Song, W., Zhao, L.: Theoretical and experimental investigations on the changing regularity of the extreme point of the temperature difference between zeotropic mixtures and heat transfer fluid. *Energy* **55**, 541–552 (2013). doi:[10.1016/j.energy.2013.02.029](https://doi.org/10.1016/j.energy.2013.02.029)
23. Klein, S.A.: *Engineering Equation Solver Academic Professional V9.459-3D. F-Chart Software* (2013)
24. Ibrahim, O.M., Klein, S.A.: Thermodynamic Properties of Ammonia–Water Mixtures. In: *ASHRAE Trans.: Symposia*; p. 21, 2, 1495–1502 (1993)
25. El-Sayed, Y.M.: On exergy and surface requirements for heat transfer processes involving binary mixtures. In: *Proceedings of ASME winter annual meeting, Chicago, 1988*. ASME-AES, vol. 6, HTD—vol. 97, pp. 19–24
26. Thorin, E.: Thermophysical properties of ammonia water mixtures for prediction of heat transfer areas in power cycles I. *Int. J. Thermophys.* **22**(1), 201–214 (2001). doi:[10.1023/A:1006745100278](https://doi.org/10.1023/A:1006745100278)
27. Neksa, P., Rekestad, H., Zakeri, G.R., Schiefloe, P.A.: CO₂-heat pump water heater: characteristics, system design and experimental results. *Int. J. Refrig.* **21**(3), 172–179 (1998)
28. Palm, B., Claesson, J.: Plate heat exchangers: calculation methods for single and two-phase flow. *Heat Transf. Eng.* **27**, 88–98 (2006)
29. Martin, H.: A theoretical approach to predict the performance of chevron-type plate heat exchangers. *Chem. Eng. Process.: Process Intensif.* **35**(4), 301–310 (1996)
30. Táboas, F., Vallès, M., Bourouis, M., Coronas, A.: Assessment of boiling heat transfer and pressure drop correlations of ammonia/water mixture in a plate heat exchanger. *Int. J. Refrig.* **35**(3), 633–644 (2012). doi:[10.1016/j.ijrefrig.2011.10.003](https://doi.org/10.1016/j.ijrefrig.2011.10.003)
31. Táboas, F., Vallès, M., Bourouis, M., Coronas, A.: Flow boiling heat transfer of ammonia/water mixture in a plate heat exchanger. *Int. J. Refrig.* **33**(4), 695–705 (2010). doi:[10.1016/j.ijrefrig.2009.12.005](https://doi.org/10.1016/j.ijrefrig.2009.12.005)
32. Táboas, F., Vallès, M., Bourouis, M., Coronas, A.: Pool boiling of ammonia/water and its pure components: comparison of experimental data in the literature with the predictions of standard correlations. *Int. J. Refrig.* **30**, 778–788 (2007). doi:[10.1016/j.ijrefrig.2006.12.009](https://doi.org/10.1016/j.ijrefrig.2006.12.009)
33. Nordtvedt, S.R.: *Experimental and theoretical study of a compression/absorption heat pump with ammonia/water as working fluid [Ph.D. Thesis]*. Norwegian University of Science and Technology (2005)
34. Silver, L.: *Gas cooling with aqueous condensation: a new procedure for calculating heat transfer coefficients*. Chemist, The Industrial (1947)
35. Bell, K.J., Ghaly, M.A.: An approximate generalized design method for multicomponent/partial condensers. In: *13th National heat transfer conference*. Denver, Colorado, USA: AIChE-ASME (1972)
36. Yan, Y., Lio, C., Lin, F.: Condensation heat transfer and pressure drop of refrigerant R-134a in a plate heat exchanger. *Int. J. Heat Mass Transf.* **42**(6), 993–1006 (1999)
37. Bejan, A.: *Advanced Engineering Thermodynamics*, 3rd edn. Wiley, New York (2006)
38. Morosuk, T., Tsatsaronis, G.: A new approach to the exergy analysis of absorption refrigeration machines. *Energy* **33**(6), 890–907 (2008). doi:[10.1016/j.energy.2007.09.012](https://doi.org/10.1016/j.energy.2007.09.012)
39. Tsatsaronis, G., Park, M.H.: On avoidable and unavoidable exergy destructions and investment costs in thermal systems. *Energy Convers. Manag.* **43**(9–12), 1259–1270 (2002). doi:[10.1016/S0196-8904\(02\)00012-2](https://doi.org/10.1016/S0196-8904(02)00012-2)
40. Ahlsell Danmark ApS. Price catalog 2013. Accessed 26 Sept 2013
41. H Jessen Jürgensen A/S: Price catalog 2013. Accessed 26 Sept 2013
42. Sørensen, K.: HPO R717 compressor cost. Personal communication 2013
43. Zamjurescu, C.: Modeling and optimization of an ammonia–water compression–resorption heat pumps with wet compression. *Trans. Can. Soc. Mech. Eng.* **33**(1), 75–88 (2009)
44. Morosuk, T., Tsatsaronis, G., Boyano, A., Gantiva, C.: Advanced exergy-based analyses applied to a system including LNG regasification and electricity generation. *Int. J. Energy Environ. Eng.* **3**, 1 (2012)

